

# Optimization Methods for Asteroid Lightcurve Inversion

## II. The Complete Inverse Problem

M. Kaasalainen, J. Torppa, and K. Muinonen

Observatory, University of Helsinki, P.O. Box 14, FIN-00014 Helsinki, Finland

E-mail: kaselain@gstar.astro.helsinki.fi

Received October 18, 2000; revised March 13, 2001

**The rotation period, pole direction, and scattering parameters of an asteroid can be deduced from its lightcurves simultaneously with the shape. Simulations and real data indicate that the result obtained with convex inversion is unique and stable if several lightcurves obtained at various geometries are available. Since the parameters of scattering laws such as the Hapke or Lumme–Bowell models cannot be determined well using lightcurves only, we introduce a simple empirical scattering law. This law can be applied in the computation of reference lightcurves and phase curves for further analysis of the physical properties of the surface. We present shape, pole, and period solutions for asteroids that have also been observed by space probes or radar.** © 2001 Academic Press

**Key Words:** asteroids, rotation; photometry; surfaces, asteroids.

### 1. INTRODUCTION

In our previous paper (Kaasalainen and Torppa 2001, hereafter Paper I) we showed that the convex hull of an asteroid can be deduced accurately from its lightcurves if the rotation parameters and scattering properties are known. Above all, we proved that the problem can be formulated such that the result is automatically realistic and still unique; numerical simulations showed that it is stable as well. Simulations also showed that nonconvex inversion is possible, although it is clearly not as stable as the convex version, nor is the result unique.

Since the optimization methods used are nonlinear, any parameters can be changed from fixed to free ones. Adding rotation and scattering to the parameter space obviously removes formal uniqueness, but one should not expect this to be an obstacle in practice. In fact, the use of relative brightnesses or a function series already removed formal uniqueness in Paper I: nevertheless, optimization always converged to the same solution. The convergence toward the correct convex shape is so robust that a few more parameters do not alter the situation locally; a grid search can be used for global scanning of the new parameters.

In Section 2 we give a concise account of the addition of rotation parameters to the optimization procedure. This addition

(as that of any other parameters) is straightforward and does not change the principles presented in Paper I in any way. In Section 3 we discuss the role of the scattering law. Inversion results for the five asteroids 243 Ida, 433 Eros, 951 Gaspra, 1620 Geographos, and 6489 Golevka are presented in Section 4. Section 5 is dedicated to conclusions and the discussion of further plans for future research and lightcurve observations.

### 2. POLE AND PERIOD

Let the pole direction of the asteroid be given by ecliptic polar angle  $\tilde{\beta}$  and longitude  $\lambda$ , and its angular rotation speed by  $\omega$ . To avoid needless confusion due to historical notation, we use the following convention:  $\tilde{\beta}$  is measured from the positive  $z$  axis and varies between  $[0, \pi]$ , and the asteroid always rotates in the positive direction (i.e.,  $\omega$  is always positive). The sense of rotation as viewed from the Earth is thus implied by  $\tilde{\beta}$ . The ecliptic latitude  $\beta$  is given by  $\beta = 90^\circ - \tilde{\beta}$ .

Let  $\mathbf{r}_{\text{ecl}}$  denote a vector in the ecliptic coordinate frame where the origin is translated to the asteroid. This vector transforms to the vector  $\mathbf{r}_{\text{ast}}$  in asteroid's own frame (where  $z$  axis is aligned with the rotation axis) by the rotation sequence

$$\mathbf{r}_{\text{ast}} = R_z(\phi_0 + \omega(t - t_0))R_y(\tilde{\beta})R_z(\lambda)\mathbf{r}_{\text{ecl}}, \quad (1)$$

where  $t$  is the time and  $R_i(\alpha)$  is the rotation matrix corresponding to the rotation of the coordinate frame through angle  $\alpha$  in the positive direction about the  $i$  axis. The angle  $\phi_0$  and the epoch  $t_0$  can be chosen at will. A practical choice (if the initial guess for the shape is an ellipsoid) is to set  $t_0$  to the time when a lightcurve observed at a small solar phase angle is at a minimum, and to set  $\phi_0$  to the azimuthal angle of the vector  $R_y(\tilde{\beta})R_z(\lambda)\mathbf{r}_{\text{ecl}}^{(E)}$ , where  $\mathbf{r}_{\text{ecl}}^{(E)}$  is the direction vector of the Earth at  $t_0$ . Thus the Earth will lie in the  $xz$  plane of the asteroid's frame at  $t_0$ , and the longest radius of the shape result is likely to be closely aligned with the  $x$  axis (provided that the initial pole is not far away from the final one).

The form (1) adds pole and period to the inverse problem in a straightforward way: the directions of the Earth and the Sun as seen from the asteroid are now simple functions of  $\tilde{\beta}$ ,  $\lambda$ , and  $\omega$ , so these parameters can readily be included in the optimization methods of Paper I. Obviously there are now several local minima in  $\chi^2$ , so the initial values for the pole and the period play a key role. The case of the pole is the simplest. We have found that it is quite sufficient to use the pole values obtained by fitting a triaxial ellipsoid. It is important to use all (typically four) poles as initial guesses, since the best ellipsoid pole is not necessarily in the correct “valley.” Another possibility is simply to use, say, a few directions in each octant of the celestial sphere as starting points; such a grid will usually cover all the local minima.

If the lightcurve set covers many years and apparitions, the period space is filled with densely packed local minima. The smallest separation  $\Delta P$  of the local minima in the trial period  $P$  spectrum of the  $\chi^2$  of the lightcurve fit is roughly given by

$$\frac{\Delta P}{P} \approx \frac{1}{2T}, \quad (2)$$

where  $T = \max(|t - t_0|)$  within the lightcurve set. This derives from the phenomenon that if  $P$  is changed by  $\Delta P$ , the minima and maxima of the model lightcurve at  $t_0 \pm T$  will undergo a phase shift of  $\pi$  so they will typically be at roughly the same places as with  $P$ . The separation  $\Delta P$  repeats over the whole of the  $\chi^2$  plot and depends only on the epochs of the lightcurves. The  $P$  spectrum is also modulated by other, longer  $\Delta P$ 's corresponding to apparition gaps shorter than  $T$ .

In principle, one should use initial periods less than  $\Delta P$  apart from each other covering the whole of the interval within which  $P$  can be expected to lie (as judged by eye from the lightcurves). In practice, only a part of this interval will be feasible a priori especially if the lightcurves are of the usual double-sinusoidal type. This part can be found by plotting  $\chi^2(P)$  using the fixed shape and pole(s) of an ellipsoidal model (Fig. 1 shows such a plot for Eros). In any case, several initial values for  $\omega = 2\pi/P$  will have to be used: the optimization procedure cannot climb out of a wrong period “ravine” even if the correct one were right next to it. This poses no practical problems, since especially the function series optimization with the Levenberg–Marquardt method (Paper I) is very fast. Thus one can easily let the procedure go automatically over hundreds of initial period values that may be needed if the lightcurve set spans a large number of years. However, the best initial values are usually found after only a few tries if an earlier model of at least some credibility is available. For this reason, we have found even crude ellipsoidal models very useful as initial guesses.

Error estimates for pole and period are not so easily obtainable. As usual, formal errors (such as the square roots of the elements of the covariance matrix) are worthless in practice since the effects of random noise are usually negligible compared to systematic and model errors. Indeed, in all our simulations even

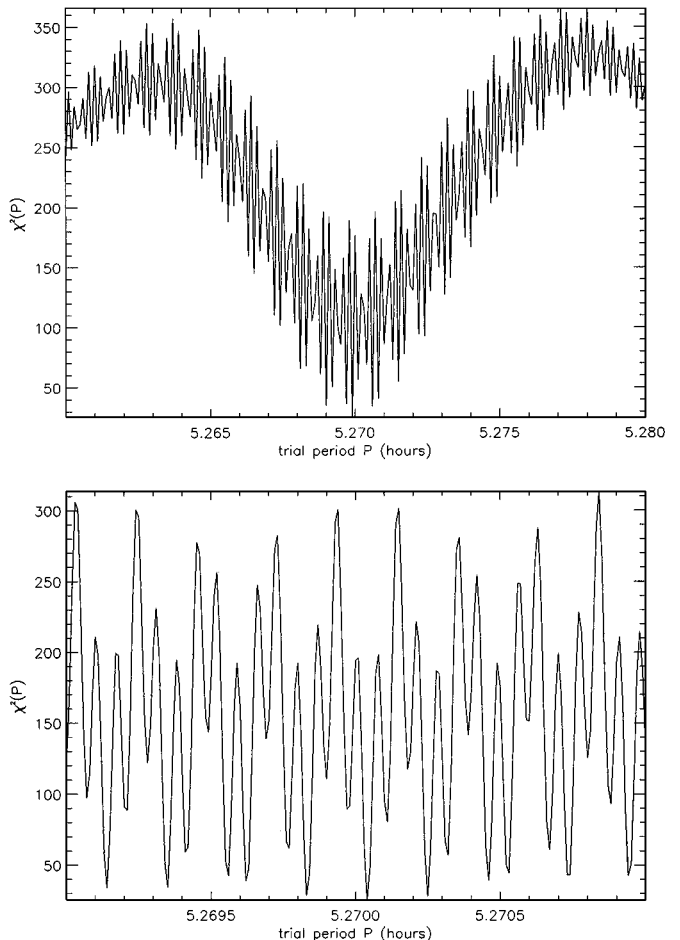


**FIG. 1.** (a) Coarse  $\chi^2(P)$  plot of an ellipsoidal model of 433 Eros (the modulations in the plot are due to the chosen sampling interval, which is longer than  $\Delta P$ ); (b) detailed  $\chi^2(P)$  plot of the best region with sampling interval less than  $\Delta P$  (now the modulations are due to the gaps between the observed apparitions in the input data).

strong noise caused only a maximum error of less than  $2^\circ$  in pole and a few thousandths of the local minimum width in period, while the shape was resolved just as well as in the simulations of Paper I. In real cases, errors usually must be larger. The only practical way of estimating them is to perform a series of optimizations with different scattering laws, optimization methods, and initial parameter values. The results with  $\chi^2$  close to the best one describe the parameter distribution. This gives at least a lower bound to the error, which is typically a few degrees for the pole.

The period error is mostly governed by the epochs of the lightcurves. If the best local  $\chi^2$  minimum of the period spectrum is clearly lower than the others, one can obtain an error estimate of, say, a hundredth part of the smallest minimum width  $\Delta P$  since the edge of a local minimum ravine always lies much higher than its bottom. Thus the period can be very accurate for data that cover many years. On the other hand, if the neighboring minima are not clearly higher than the best one, the

accuracy cannot be considered better than  $\Delta P$  since the local error estimate cannot be applied globally (this is why many formal period errors reported in asteroid literature are much too small). This may happen if, for example, there are only two well-observed apparitions available, so the exact number of asteroid revolutions between the apparitions is uncertain. The more apparitions there are available, the more pronounced the correct local minimum is; our method thus automatically combines all apparitions and observations to improve the period estimate.

The above analysis applies to asteroids in relaxed rotation. If the asteroid is precessing, only a few more parameters are added to the problem, and it seems that the feasible regions of parameter values can be found quite fast. We are currently experimenting with different methods to solve for the rotational state of a freely precessing asteroid. Our studies indicate that asteroid lightcurves are so strongly defined by the convex hull and the rotation of the asteroid that convergence toward the correct minimum can usually be expected to be robust (Kaasalainen (2001)).

### 3. SCATTERING LAW

There are currently no scattering models that could adequately explain the scattering behavior of asteroid surfaces. For example, the models by Hapke or Lumme and Bowell (see the review by Bowell *et al.* (1989)) are notorious for producing ambiguous and unrealistic parameter values in inverse problems (see, e.g., Karttunen and Bowell (1989)). Moreover, they cannot fully account for the opposition effect mainly caused by two mechanisms: coherent backscattering and shadowing (e.g., Muinonen (1994), and references therein). Indeed, it is precisely the opposition effect that often forces us to use relative brightnesses already in theory: if the effect of solar phase angle on surface brightness cannot be modeled accurately, fitting absolute brightnesses is useless. This problem is further exacerbated by the unfortunate

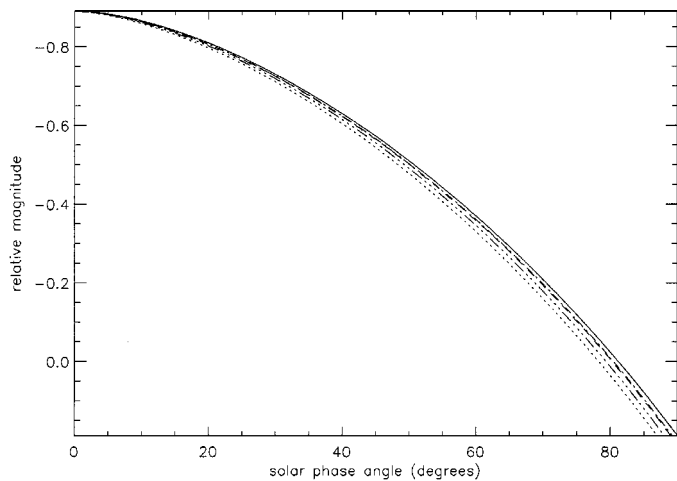


**FIG. 2.** Reference phase curves  $\mathcal{R}(\alpha)$  of substantially nonconvex shapes (dashed lines) and of a sphere (solid line); the scattering law is (3) with  $c = 0.1$  and  $f(\alpha) = 1$ .

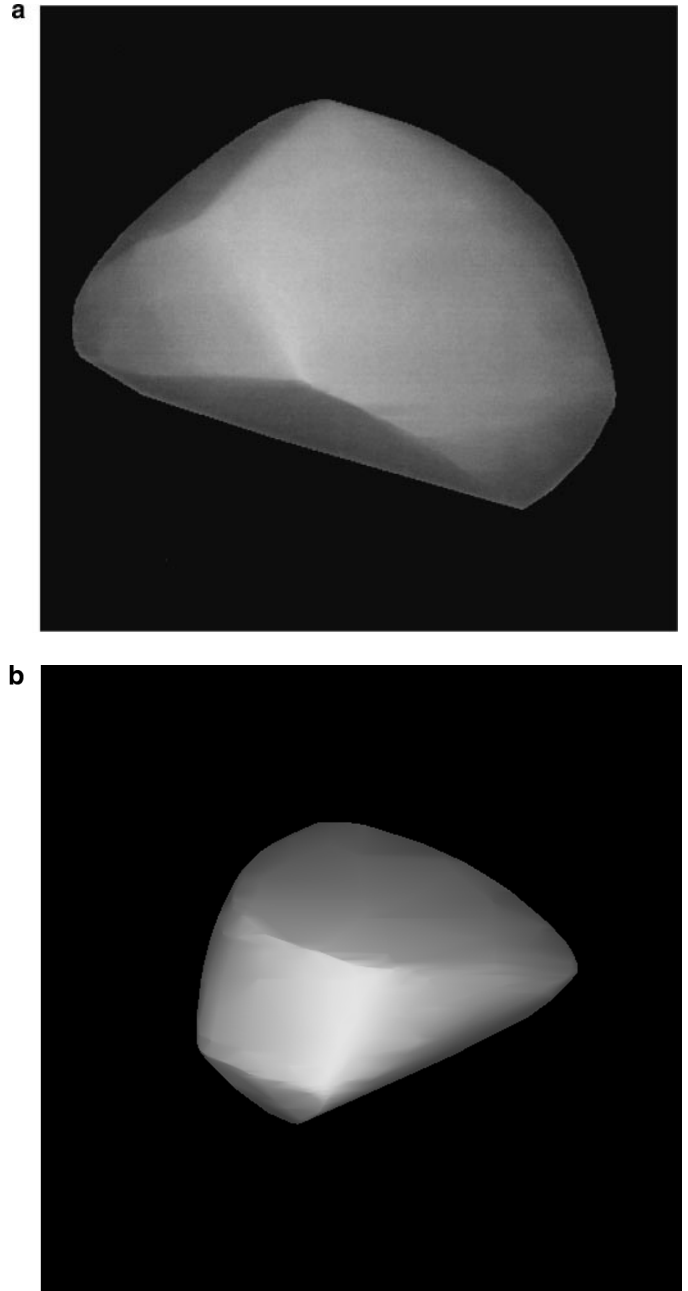


**FIG. 3.** Convex shape model of 6489 Golevka, seen and illuminated from two directions:  $(\theta, \phi) = (-25^\circ, 70^\circ)$  and  $(\theta, \phi) = (15^\circ, 225^\circ)$ .

fact that the absolute brightnesses of observations are often not known accurately enough: to obtain proper line-over-points fits, the relative  $\chi_{\text{rel}}^2$  of Paper I may sometimes be the only possibility.

For lightcurve inversion, the scattering law must be simple: too many parameters and possibilities cause instability and unrealistic results. According to our experience, the scattering law can well be simpler than, e.g., the Lumme–Bowell and Hapke laws that aim to account for certain physical properties of the surface. Our main idea is to avoid detailed physical parameters and simply to try to describe the general photometric properties of the surface.

While striving toward a simple scattering law, the model must still be chosen realistic enough. We make use of

$$\begin{aligned} S(\mu, \mu_0, \alpha) &= f(\alpha)[S_{LS}(\mu, \mu_0) + cS_L(\mu, \mu_0)] \\ &= f(\alpha)\mu\mu_0\left(\frac{1}{\mu + \mu_0} + c\right), \end{aligned} \quad (3)$$

which combines single (Lommel–Seeliger term  $S_{LS}$ ) and multiple scattering (Lambert term  $S_L$ ) with a weight factor  $c$  for the latter. For the sake of convenient inversion, the phase function  $f(\alpha)$  is taken to multiply the sum of the single- and multiple-scattering terms. Such a simplification can be justified by the ambiguity in what should be called single or multiple scattering in a particulate medium consisting of small particles that are, to an extent, aggregates of even smaller particles.

When relative brightnesses are used in inversion, we automatically obtain a scale factor a posteriori for each lightcurve by dividing the average observed brightness by the corresponding

model brightness (when other, trivial scale factors such as distances have been corrected for). We can then obtain the phase function  $f(\alpha)$  by fitting, e.g., a simple exponential and linear model to the scale factors. This has proven to be a versatile choice when modeling the intensity of scattered light as a function of phase angle (cf. S. Kaasalainen *et al.* (2001) and references therein), but we emphasize that any other function can be used without altering the pole/shape result in any way. Since  $f(\alpha)$  can be multiplied by any constant (when the absolute scales of the size and darkness of the asteroid need not be fixed), we can normalize the linear part to unity at opposition after the fit to be able to compare the shapes of different phase functions. Thus we report  $f(\alpha)$  in the three-parameter form

$$f(\alpha) = A_0 \exp\left(-\frac{\alpha}{D}\right) + k\alpha + 1, \quad (4)$$

where  $A_0$  and  $D$  are the amplitude and scale length of the opposition effect, and  $k$  is the overall slope of the phase curve. The final

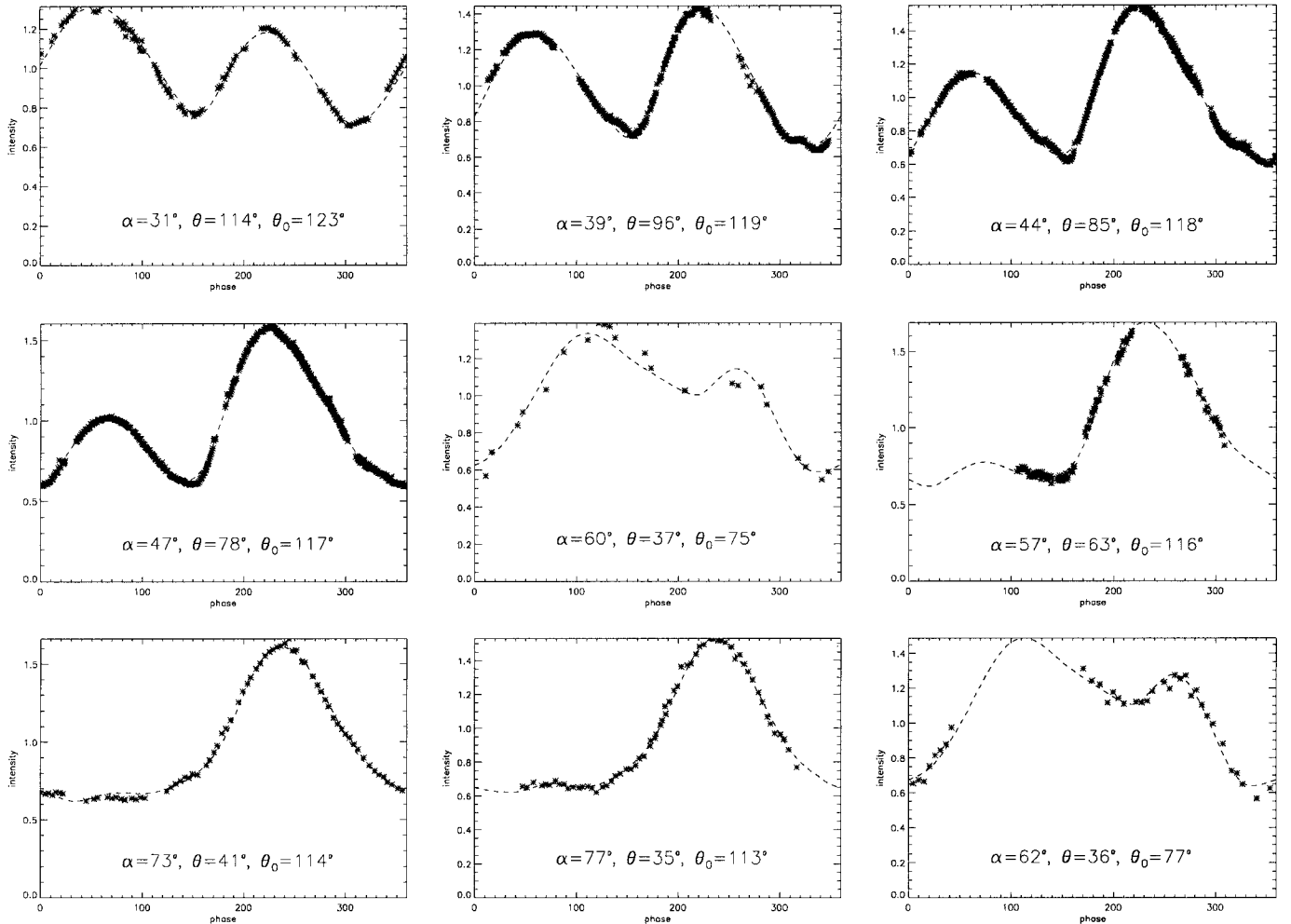


FIG. 4. Typical lightcurve fits for 6489 Golevka. The observed brightnesses are shown as asterisks, and the model brightness is shown as a dashed line.

scattering law has now only four parameters, and only one of them (the Lambert weight) is optimized in lightcurve inversion.

Note that the present empirical modeling does not require hypotheses about the physics behind the opposition effect. In fact, we do not have to know anything about the opposition effect, not even whether it exists in the first place: if (4) does not fit the scale factors well, we can use any other function or just plot the points as such.

We have found that Hapke, Lumme–Bowell, and the above scattering model all give very closely the same results for the shape and the rotational state; examples of this are shown in Section 4. When the two first scattering laws are used in conjunction with the relative  $\chi_{\text{rel}}^2$ , a further constraint is introduced: the scale factors for a given wavelength (different colors having somewhat different scattering properties) should remain constant by definition (as no  $f(\alpha)$  is used) since otherwise the fitted law would be meaningless. Thus the scale factors must be added to the inversion procedure as a regularization function in the form of an additional model “curve.” This usually succeeds well at least at solar phases not very close to opposition; at smaller phase angles, the scattering law must be able to describe the opposition effect well. Often some of the parameters must be fixed a priori for a stable solution, and the allowed intervals of the others must be restricted in the same way as albedo in Paper I since typically the numerically best fit is obtained at physically very peculiar parameter values.

Whatever the parameters and functional form of the scattering law, the inversion result is only an empirical fit: the final values of physical scattering parameters should never be taken too seriously. In view of the above we conclude that, for inversion purposes, it may sometimes be better to avoid “physical” scattering models altogether. The drawbacks of an empirical model are that it can seldom be used for extrapolation in solar phase angle, and the points to be fitted must be dense for proper interpolation. In the case of (4), for example,  $f(\alpha)$  may reach negative values at phase angles much larger than those of the observations, and the description of the opposition effect is not accurate if there are not enough lightcurves at small phase angles. Physical models usually constrain the shape of the phase curve more efficiently with fewer points.

### 3.1. Reference Phase Curves

Once the scattering law, shape, and the rotation period and pole are known for the asteroid, we can compute “reference lightcurves and phase curves” as functions of solar phase angle in a partially fixed illumination and observation geometry, i.e., in a “reference geometry.” Equatorial illumination and viewing is a natural choice for this purpose. It is highly plausible that such reference curves depend very little on the detailed scattering law utilized in inversion: since the scattering law is employed twice, in inversion and subsequent direct computation, errors in the simple scattering law tend to cancel each other, so the reference lightcurves should well represent observations made at arbitrary geometries.

We define the reference phase curve  $\mathcal{R}(\alpha)$  as the intensity time average of the lightcurve generated in the reference geometry at solar phase angle  $\alpha$  (to conform with the established practice of portraying phase curves, we use magnitude units when plotting  $\mathcal{R}$ ). Such well-defined phase curves can be applied in further detailed studies of asteroid surfaces; these curves are considerably more reliable than the traditional badly defined curve fits obtained directly from observed magnitudes (often questionably

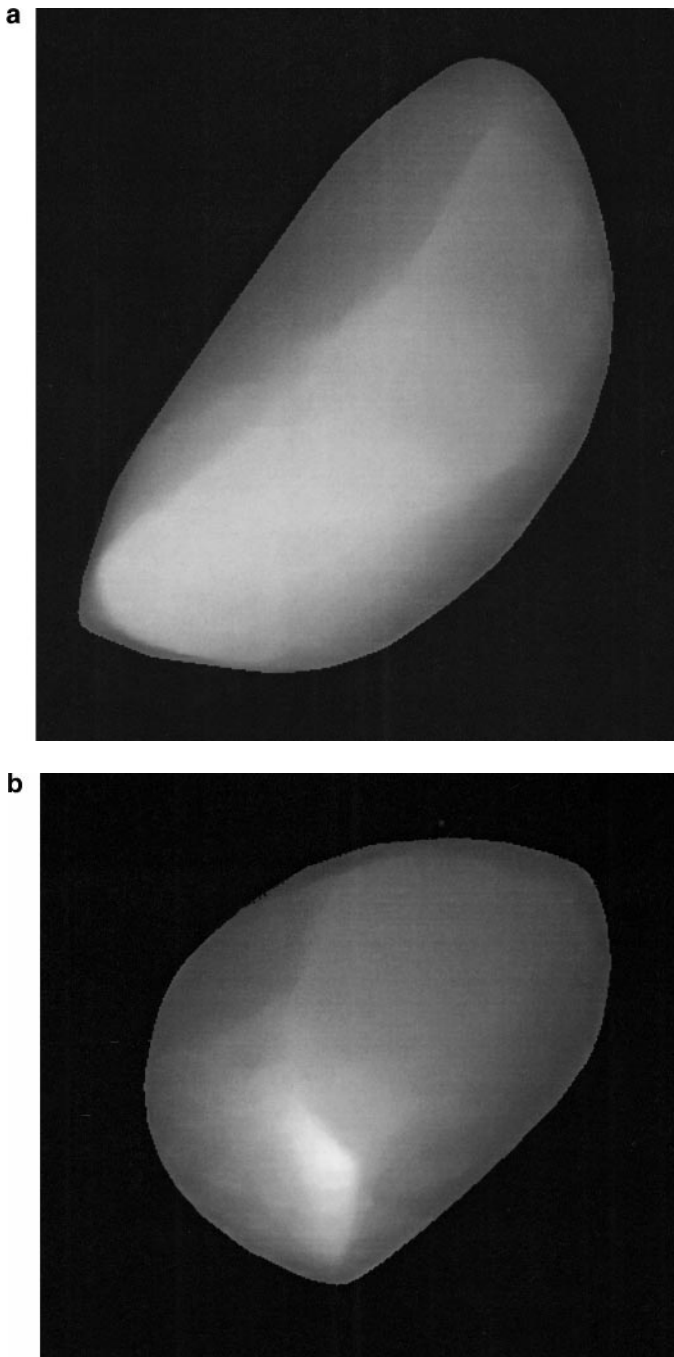


FIG. 5. Convex shape model of 433 Eros, seen and illuminated from two directions:  $(\theta, \phi) = (50^\circ, 10^\circ)$  and  $(\theta, \phi) = (20^\circ, 190^\circ)$ .

reduced without a proper shape model). One can also compute any other characteristic quantities, e.g., the amplitude–phase relationship, just as easily.

We have found that, unlike phase curves at nonequatorial geometries (not to mention plots of maxima or minima), the reference phase curve is remarkably insensitive to the shape of the asteroid. In the Appendix we show that the reference phase curves of convex bodies are actually completely independent of the shape for some scattering laws. This property is quite welcome as a separating tool: the information on large-scale features and separate details (that would be distinctly visible in a disk-resolved image) is virtually lost at the phase curve stage, leaving only the statistical small-scale properties to be inferred. Our simulations with irregular shapes show that large-scale nonconvexities do not affect the phase curve significantly: it is precisely the small-scale roughness that causes the darkening at growing phase angles, not the shadows of macroscopic topographic features. The scale from roughness to topographic nonconvexities is, of course, a continuum; we intend to study where exactly, in the

photometric sense, the transition zone between the two regions lies.

A typical result is shown in Fig. 2. The reference phase curves of the nonconvex shapes of Paper I as well as the Gaspra shape of this paper are plotted for the scattering law (3) with  $c = 0.1$  (and  $f(\alpha) = 1$  for simplicity), all normalized to start from the same point at opposition. The phase curve of a sphere is plotted as well: the phase curves of the convex hulls of the shapes (or of any other convex shapes such as bricks, ellipsoids, or pyramids) follow the sphere’s curve very accurately, and match it exactly if  $c = 0$  (see Appendix). Obviously the effects of even strong concavities are practically negligible. Roughly speaking, if an observed phase curve drops, say, some two magnitudes between opposition and  $\alpha = 60^\circ$ , then the  $f(\alpha)$  part contributes about 1.3 mag to the darkening, the decreased illumination of the disk accounts for about 0.6 mag, and the darkening due to macroscopic nonconvex shadowing is typically responsible for less than 0.1 mag.

The empirical model (4) is remarkably versatile for a few-parameter model; as will be shown in Section 4, it can mimic,

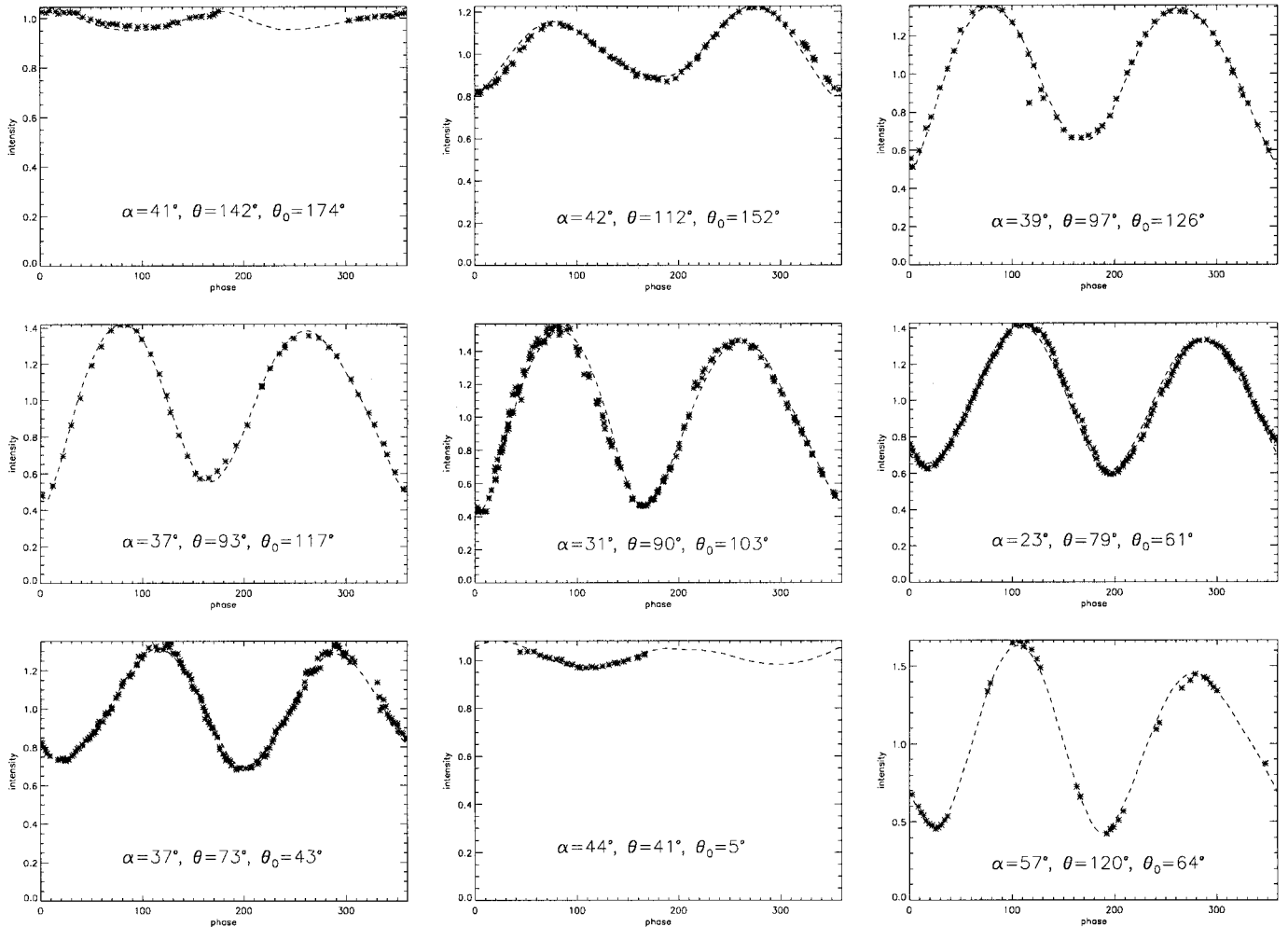


FIG. 6. Typical lightcurve fits for 433 Eros. The observed brightnesses are shown as asterisks, and the model brightness is shown as a dashed line.

e.g., Hapke phase curves very closely. We thus believe that, within observational uncertainties, the empirical approach to phase function modeling is wholly justifiable at least for classification purposes.

#### 4. RESULTS FOR FIVE ASTEROIDS

In the following, we report inversion results for five asteroids of which there are plenty of lightcurves as well as probe or radar images. The qualitative comparison of the differences between the shapes obtained for a single asteroid with different scattering laws or parameters would require a lot of page space filled with images that are practically copies of each other. Therefore we use  $\Delta\rho$  introduced in Kaasalainen *et al.* (1992) as a quantitative measure of the difference between two shapes.

If the centroids of the two body shapes are translated to the origin, and their volumes are scaled to be the same,  $\Delta\rho$  is given by

$$\Delta\rho = \frac{1}{4\pi} \sum_i \frac{|\rho_i^{(A)} - \rho_i^{(B)}|}{\rho_i^{(A)}} \Delta\sigma_i, \quad (5)$$

where  $A$  and  $B$  refer to the two shapes,  $\rho_i$  is the distance of facet  $i$  from the origin, and  $\Delta\sigma_i$  is the area of the triangle on the unit sphere that determines the direction of the surface normal of facet  $i$ . This measure is stable and reflects the difference between two shapes rather well. (When  $\Delta\rho$  is small, the asymmetry of the measure with respect to  $A$  and  $B$  is insignificant.)

The scale for  $\Delta\rho$  is roughly as follows:  $\Delta\rho \leq 2\%$ , practically the same shape;  $\Delta\rho \leq 4\%$ , the shapes resemble each other very closely;  $\Delta\rho \leq 6\%$ , the shapes are quite similar;  $\Delta\rho \leq 8\%$ , the shapes are roughly similar;  $\Delta\rho \leq 10\%$ , the shapes have similar general dimensions. As a rule,  $\Delta\rho$  between the best ellipsoid and the general convex result is about 10% or more. A somewhat surprising finding is that the shapes obtained with three different scattering laws are typically within  $\Delta\rho$  of only a few percent. From this we can deduce that lightcurves indeed constrain the possible convex hull of the object very strongly.

The deviation of the lightcurve fits is computed from  $\sqrt{\chi_{\text{rel}}^2/N}$ ; i.e., the mean brightness of each observed lightcurve is scaled to unity. Note that the lightcurve plots describe intensities, not magnitudes. The plots are given as functions of the synodic rotational phase, i.e., the opposite of the azimuthal angle of the Earth as seen from the asteroid. The solar phase angle  $\alpha$  as well as the aspect angles for the Earth ( $\theta$ ) and the Sun ( $\theta_0$ ) are reported for each lightcurve. Our error estimates for pole and period describe the deviation between results for different scattering laws and initial values, so they should be taken as lower bounds of the real errors.

All the lightcurves used in inversion were obtained from the *Uppsala Asteroid Photometric Catalogue* (UAPC; Lagerkvist *et al.* 1996, 2001). Some lightcurves contain hundreds of points,

while most have 30–70 and some only a few; also, some dates may be represented more heavily than others. This is a potential source of biasing effects; however, visual checking of plots shows whether some lightcurves have been unduly favored at the expense of others, and separate weighting factors (also taking into account the quality of the lightcurves) can be applied. So far we have not found any such factors necessary, but it is sometimes expedient simply to remove redundant or bad lightcurves from the data set. As there was no shortage of data in any of the five cases presented here, we decided to use only the best observations (later checking that the inversion results fit the leftover data as well).

Although we used three scattering laws—Hapke, Lumme–Bowell, and the empirical model—in all cases, we purposely do not report the detailed parameters of the first two lest too much importance should be attached to them. The different scattering

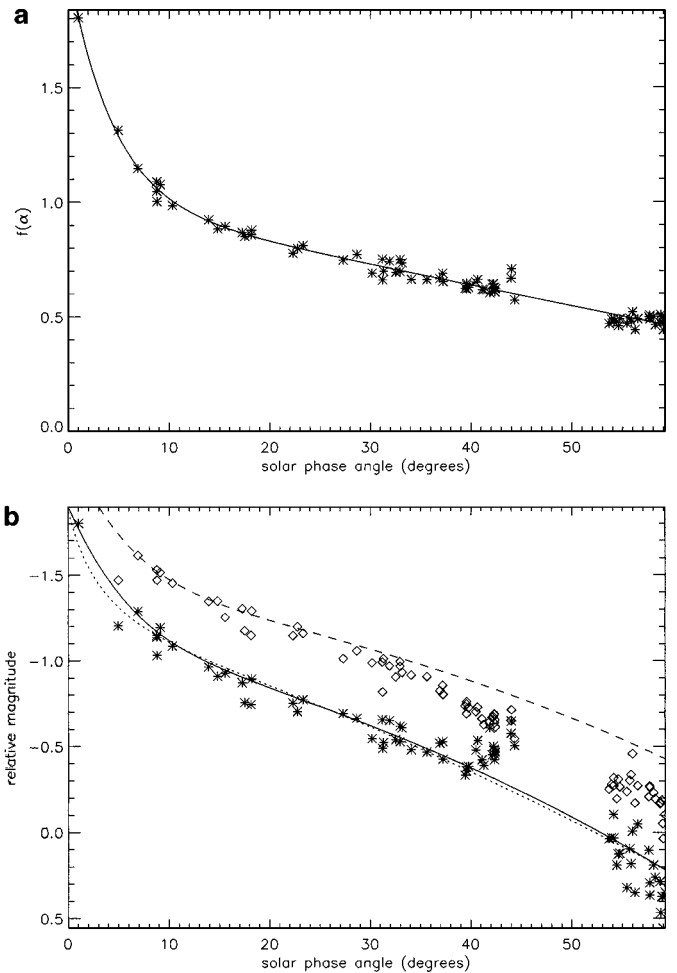


**FIG. 7.** (a) The phase function  $f(\alpha)$  for 433 Eros; (b) the corresponding reference phase curve  $\mathcal{R}(\alpha)$  for Eros (solid line), together with the phase curve obtained with the best-fit Hapke parameters (dotted line), and the computed maxima at the reference geometry (dashed line). Observed average brightnesses are plotted with asterisks, and the observed maxima with diamonds (note the displacing effect of nonreference geometries).

models serve best to give error estimates for all other optimized parameters; a stable representation of an object’s scattering behaviour is, e.g., the reference phase curve (of which we give an example for 433 Eros). The model images are displayed at opposition with an artificial “revealing” scattering law for visualization purposes. The viewing latitude is given by  $\theta$  and longitude by  $\phi$ . In order to keep the paper compact, we do not show multiple views or sequences; we are planning an electronic library (accessible via Internet) for full 3-D models and graphics packages for viewing/illumination in, e.g., observational lightcurve geometries. Examples of such animations can be found in Kaasalainen *et al.* (2001) (<http://epubs.osa.org/opticsexpress/>).

#### 4.1. 6489 Golevka

6489 Golevka is in many ways a model example of a well-observed asteroid and a rich lightcurve set, proving that only a few months’ observation campaign can provide enough data for a detailed analysis of a near-Earth object. Our data set consisted of 32 lightcurves with solar phases as large as  $81^\circ$ , mea-

sured between April and August 1995. Since the observations are from one apparition only, the typical thicket of local minima in the  $\chi^2(P)$  plot is absent. Therefore one local minimum covers the whole of the feasible period region, so the procedure finds the best period with any initial guess. The solutions obtained with different scattering laws/parameters differ from each other very little;  $\Delta\rho$  between comparison pairs ranges from 1.5 to 3.5%, while for the best ellipsoid vs others  $\Delta\rho > 10\%$ .

The shape result and some interesting input lightcurves are shown in Figs. 3 and 4. The lightcurves were fitted within less than 3% deviation (0.03 mag). Note that the convex model reproduces all lightcurve features accurately. The shape result shows that Golevka is clearly a very irregular body with sharply defined edges. Golevka is also in other respects an example of an asteroid that cannot be modeled with an ellipsoid: the correct pole is in the direction opposite to that estimated by Mottola *et al.* (1997); i.e., the rotation is retrograde rather than prograde. Our shape model agrees well with the radar model by Hudson *et al.* (2000).

For Golevka’s period we obtain  $P = 6.0297 \pm 0.0001$  h, which is a few seconds longer than the  $6.0289 \pm 0.0001$  h by

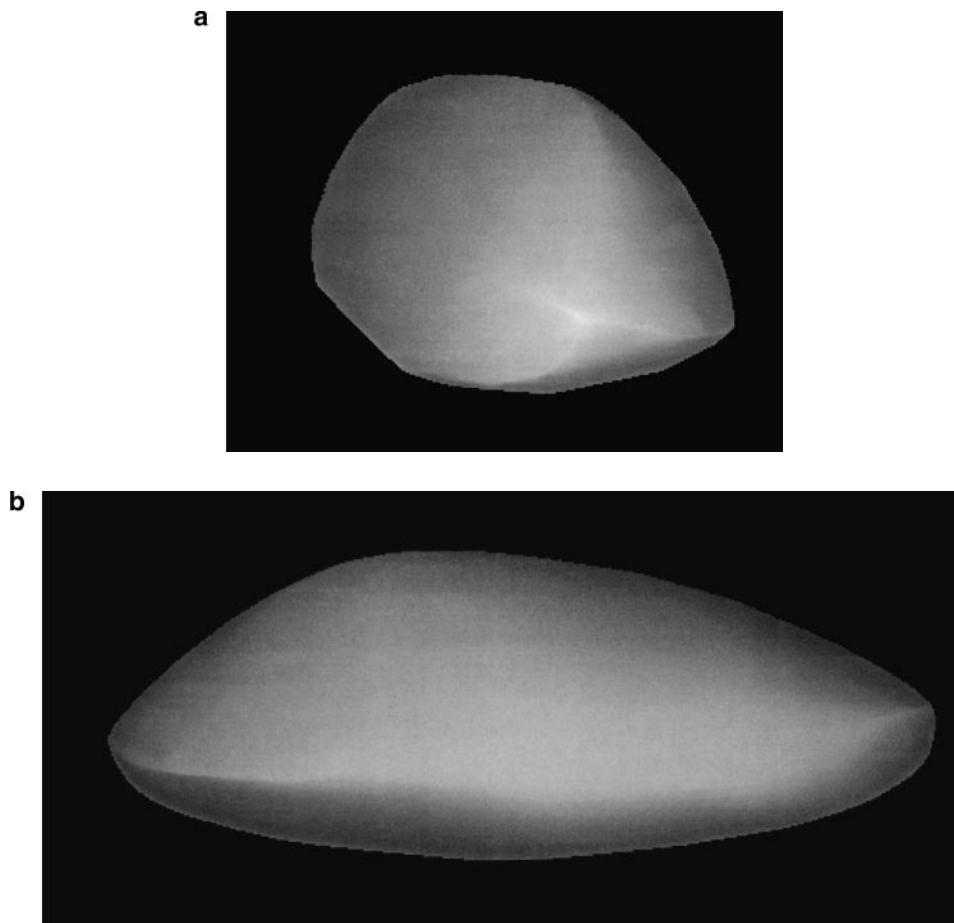


**FIG. 8.** Convex shape model of 1620 Geographos, seen and illuminated from two directions:  $(\theta, \phi) = (10^\circ, 160^\circ)$  and  $(\theta, \phi) = (0^\circ, 270^\circ)$ .

Hudson *et al.* (2000). The pole is at  $\lambda = 208 \pm 3^\circ$ ,  $\beta = -47 \pm 4^\circ$ , a few degrees away from  $\lambda = 202 \pm 5^\circ$ ,  $\beta = -45 \pm 5^\circ$  obtained by Hudson *et al.* (2000). Numerically the best fits (the difference in  $\chi^2$  having no statistical significance) were obtained with (3) ( $c = 0.3$ ) and the Lumme–Bowell law. Since we were mostly interested in the shape and the rotational state of the object, and no absolute magnitudes were reported for our data set at small solar phases (and those reported for the leftover data were not very accurate), we did not study the details of the scattering behavior near opposition. Roughly speaking, the parameters of (4) are  $A_0 \approx 0.6$ ,  $\mathcal{D} \approx 4^\circ$ ,  $k \approx -0.007$ . In all cases, albedo effects (Paper 1) were negligible or very small, having no effect on the shape result.

#### 4.2. 433 Eros

433 Eros is one of the longest and the best-observed asteroids, now thoroughly mapped by NEAR Shoemaker (Veverka *et al.* 2000). We used a data set of 78 lightcurves reaching solar phases

up to  $59^\circ$ , measured between 1951 and 1993 (the great majority during the 1974–1975 apparition). The initial scan of the  $\chi^2(P)$  plot of an ellipsoidal model (Fig. 1b) showed many possible initial period values; the final local minimum of the best solution stood out quite clearly. All shape results fitted within  $\Delta\rho = 2\%$ , while between these and the best ellipsoid  $\Delta\rho = 9\%$ . The shape result and some input lightcurves are shown in Figs. 5 and 6. The fit with the Hapke law and scale factor regularization was, as usual, ambiguous: many possible parameter sets gave equally good fits. As good a  $\chi^2$  was also obtained with (3) and  $c = 0.1$ . For the period we obtained  $P = 5.2702528 \pm 0.0000002$  h, and the pole is at  $\lambda = 16 \pm 1^\circ$ ,  $\beta = +9 \pm 2^\circ$ , coinciding accurately with the pole from probe images. For Eros, the separation of the local  $\chi^2(P)$  minima is about 0.00007 h; within the best local minimum practically all initial values and optimization techniques indeed lead to periods within much less than a hundredth part of the local valley’s width—hence our extremely small error estimate. To be more on the safe side, we estimate  $P = 5.2702528 \pm 0.0000007$  h.

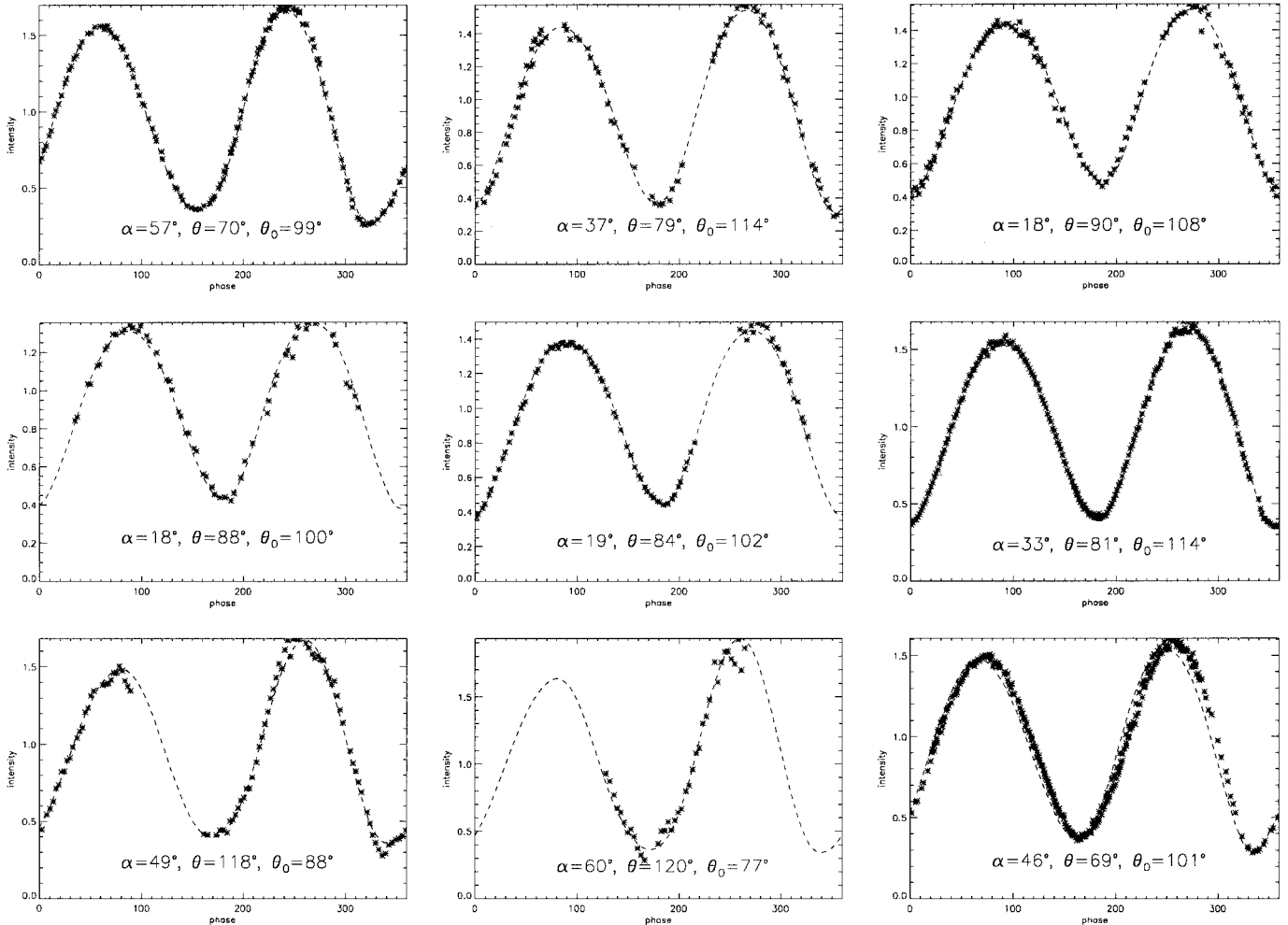


FIG. 9. Typical lightcurve fits for 1620 Geographos. The observed brightnesses are shown as asterisks, and the model brightness is shown as a dashed line.

The lightcurves were fitted within 6% deviation, most of which is due to the early lightcurves that clearly contain large systematic photometric errors; the majority of the lightcurves were fitted within 3%. Some later lightcurves also have systematic errors apparently due to erroneous timing or data reduction. It is surprising how little effect the sizable surface concavities have on the shapes of the lightcurves. No specific features are seen, and all lightcurves are well explained by the convex model that very much looks like the probe image of Eros wrapped in gift paper: the long, straight side of the convex shape betrays the existence of the now well-known banana-shaped indentation below.

Eros is a prime example of how the convex hull of an asteroid defines the lightcurves even at large solar phase angles. Indeed, so far we have not seen a single distinct lightcurve feature that could not be explained by a convex shape. The banana shape was reproduced in some of our nonconvex inversion solutions, but not conclusively. This point will be discussed in more detail below after the analyses of the sample asteroids.

In Fig. 7a we show the phase function  $f(\alpha)$  of (4) fitted to the obtained scale factors ( $A_0 = 1.0$ ,  $\mathcal{D} = 4.5^\circ$ ,  $k = -0.009$ ), and in Fig. 7b the corresponding reference phase curve (solid line). For comparison, we also show the curve of the computed maxima as well as the observed averages (asterisks) and maxima (diamonds). The effect of the difference between observing and reference geometries is clearly seen, and the widening gap between the curves of averages and maxima defines the amplitude–phase relationship. The reference phase curve obtained with the best-fit Hapke model (shown in dots), whose parameters were constrained to typical values, follows the solid line in close agreement; note that the two curves are obtained from two independent optimizations of shape, pole, and scattering model. Because of the ambiguity problem of Hapke modeling, the phase curves of many outlandish Hapke solutions are very similar to that of the solution with typical parameter values. Although unambiguous, the empirical  $f(\alpha)$  is somewhat uncertain because of the noise and scarcity of input scale factors at small phase angles; it is, in fact, possible to fit  $f(\alpha)$  such that its  $\mathcal{R}(\alpha)$  matches the Hapke curve even more accurately while still fitting the scale factors very well.

The absolute brightnesses of the model lightcurves, computed after the  $\chi_{\text{rel}}^2$  fit using the estimated  $f(\alpha)$  or Hapke parameters, match the observed ones well with an average deviation of less than 0.05 mag. It is also interesting to note that the absolute brightnesses from the two scattering laws differ from each other only 0.02 mag on average. We can thus see that, in addition to reproducing both the shapes and the absolute magnitudes of the lightcurves well, two independent optimizations with different scattering models yield almost identical descriptions of the shape, rotational state, and photometric properties of object.

#### 4.3. 1620 Geographos

The lightcurves of 1620 Geographos can also be modeled very well with a convex shape (Figs. 8 and 9). All three scattering

models fitted the observations (35 lightcurves,  $\alpha < 57^\circ$ , measured mostly, 1993–1994—only a few in 1969 and one in 1983) within 3% deviation (0.03 mag). The difference  $\Delta\rho$  between the corresponding shape models was less than 5%. The slightly expanded elbow room for the shape result (as compared to the previous examples) is caused by the narrow latitude coverage of observing geometries, restricted to equatorial aspects. In this case the initial ellipsoid is already a good guess, since the difference  $\Delta\rho$  between it and the others is only slightly over 6%. Again, our model agrees well with that by Hudson and Ostro (1999).

The period is  $5.2233260 \pm 0.0000008$  h, and the pole is at  $\lambda = 55 \pm 3^\circ$ ,  $\beta = -45 \pm 3^\circ$ . The phase dependence of light scattering cannot be determined well as there are no observations below  $11^\circ$  solar phase, and there is proper coverage only after  $\alpha > 17^\circ$ . For this asteroid, both Lumme–Bowell and Hapke laws fitted the lightcurves slightly better than (3), and the corresponding shape results were closer to the radar model. Normal parameter values could, however, be obtained only by severely constraining most of the parameters to values such as those in Hudson and Ostro (1999).

#### 4.4. 951 Gaspra

Asteroid 951 Gaspra is an example of an asteroid with a large yet insufficient lightcurve data set (48 lightcurves,  $\alpha < 25^\circ$ ,

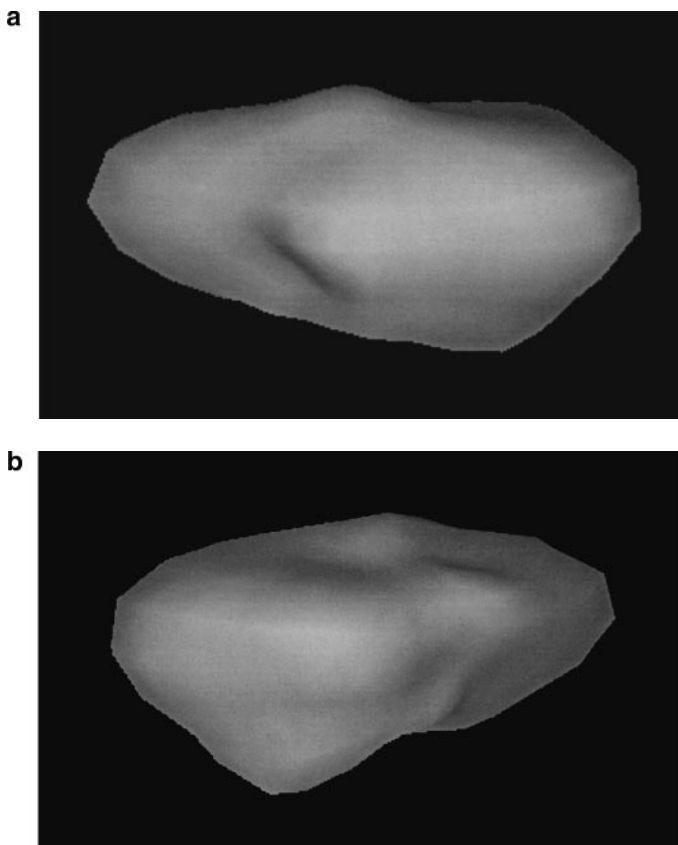


**FIG. 10.** Nonconvex shape model of 951 Gaspra, seen and illuminated from two directions:  $(\theta, \phi) = (15^\circ, 90^\circ)$  and  $(\theta, \phi) = (0^\circ, 230^\circ)$ .

measured 1988–1991, almost all during the apparitions of 1990 and 1991). None of the lightcurves at our disposal were observed below  $20^\circ$  north of the equator level; i.e., a large portion of the southern hemisphere remained unseen. This made the shape result uncertain even though pole and period seem to be well defined, with  $P = 7.04206 \pm 0.00002$  h and  $\lambda = 20 \pm 3^\circ$ ,  $\beta = +19 \pm 3^\circ$ , only a tenth of a second and  $2^\circ$  away from the *Galileo* values. The inversion result fits the lightcurves within 2% deviation (0.02 mag). For Gaspra, the parameters of (4) are about the same as for Golevka, with slightly smaller  $A_0 \approx 0.5$  and steeper  $k \approx -0.01$ .

To illustrate a typical result of nonconvex inversion, we show in Fig. 10 a nonconvex shape result for Gaspra obtained without any regularization; some lightcurve fits are shown in Fig. 11. It must be stressed that this solution is not unique, and that a convex solution gives as good a  $\chi^2$ . Also, the lowest parts of the southern hemisphere are only defined by extrapolation via the spherical harmonics series. With different smoothness regularizations or initial guesses we obtain differently undulating

surfaces and practically the same  $\chi^2$ . However, all results do exhibit some of the major nonconvex features seen in *Galileo* images. Simulations (such as in Paper I) indicate that such persistent features may have statistical significance; we return to this below.

#### 4.5. 243 Ida

243 Ida proved to be an interesting case. Although Ida is a well-observed asteroid, the data set (40 lightcurves,  $\alpha < 21^\circ$ , measured 1988–1993) admits two pole solutions (obviously due to restricted observing geometries), both of which fit the observations very well (within 3.5% deviation). Typical lightcurve fits are shown in Fig. 12. The data could not constrain the latitude of the local poles very accurately either: the two possible solutions are at  $\lambda_1 = 262 \pm 3^\circ$ ,  $\beta_1 = -55 \pm 10^\circ$  and  $\lambda_2 = 85 \pm 3^\circ$ ,  $\beta_2 = -47 \pm 5^\circ$ , while the pole from *Galileo* images is estimated at  $\lambda = 262^\circ$ ,  $\beta = -67^\circ$ . For the period we obtained  $P = 4.633638 \pm 0.000002$  h.

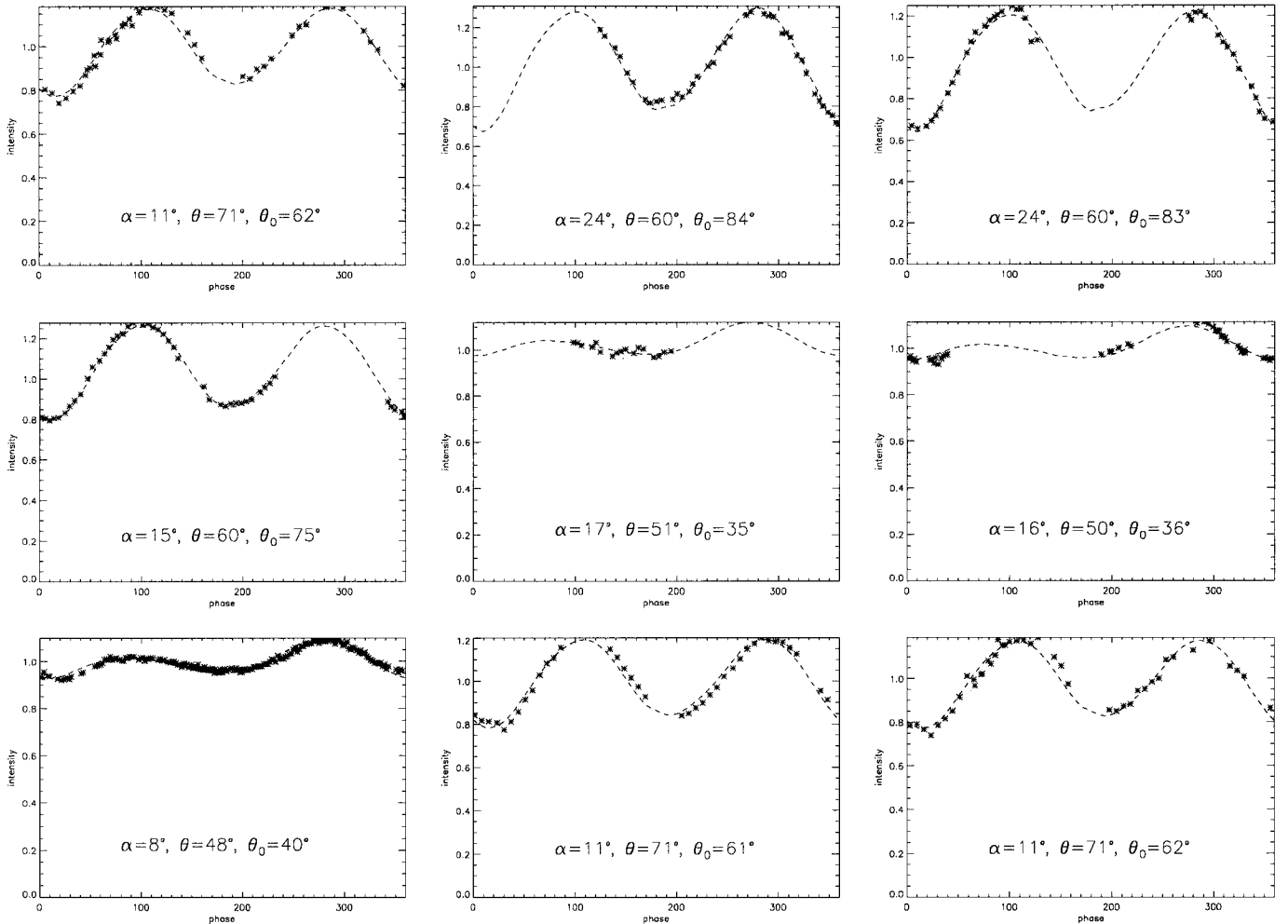
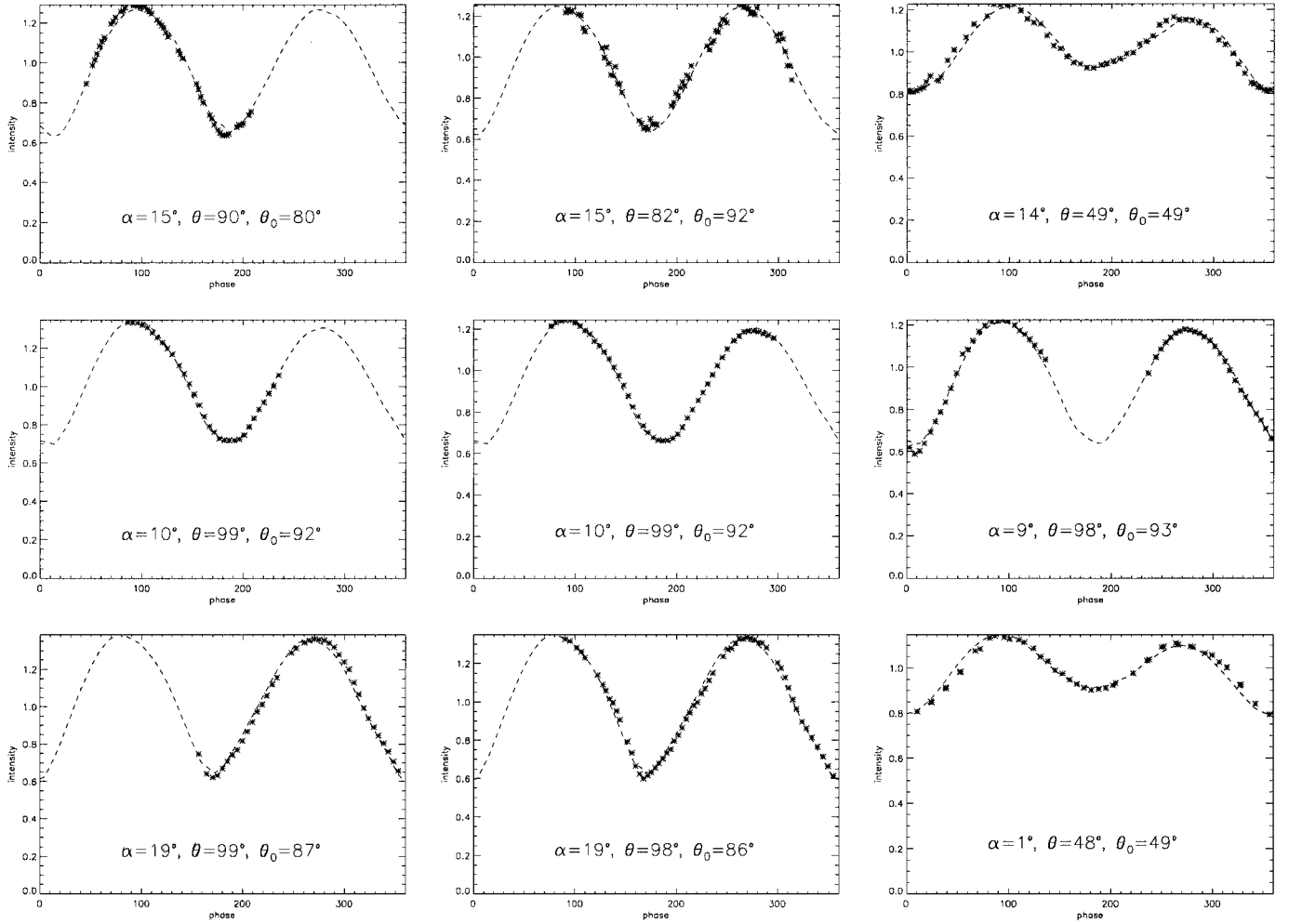


FIG. 11. Typical lightcurve fits for 951 Gaspra. The observed brightnesses are shown as asterisks, and the model brightness is shown as a dashed line.



**FIG. 12.** Typical lightcurve fits for 243 Ida. The observed brightnesses are shown as asterisks, and the model brightness is shown as a dashed line.

Because of the two possible poles, no quantitative details of the shape can be inferred. Judging from lightcurves only, we would have to content ourselves with reporting the basic dimensions of the object despite some qualitative similarities between the two model shapes. Since there are probe images of Ida, we show a nonconvex shape result for the correct pole (Fig. 13) to illustrate an important point discussed next.

#### 4.6. Photometric Convex Hull and Stability

As described in Paper I, the strong stability of the Minkowski problem makes convex inversion robust. The convex shape result is not exactly the convex hull but a shape close to it, “trimmed” such that its shadowing properties mimic those of the nonconvex shape best. In other words, the basic convex shape of which the nonconvexities could be seen as “deviations” is not the convex hull but something closely related to it; we call this basic shape the photometric convex hull of the body. Minkowski stability means that the “trimmings” may be considerable in the local

surface curvature but do not influence the global shape of the photometric convex hull very much.

For example, the Ida model of Fig. 13 produced a  $\chi^2$  slightly higher than that of the convex result even though this shape mimics some of the features of the shape model from *Galileo* images. In fact, even if one uses the correct nonconvex shape and pole, the observed lightcurves are not fitted any better than with the photometric convex hull because of observational errors and the necessarily inadequate scattering model. Thus it is not surprising that our fits are better than those of Simonelli *et al.* (1995, 1996), who only fitted Hapke parameters using the asteroid shape and pole already known from flybys. The photometric convex hull is usually a stable inversion result, whereas any nonconvex shape solution obtained from lightcurves alone is, at best, an educated guess.

Figure 13 is an example of an educated guess: the nonconvex solution was obtained by using a low-order function series fitted to the vertices of the photometric convex hull as the initial shape for iteration. This procedure can, in a way, interpolate the convex

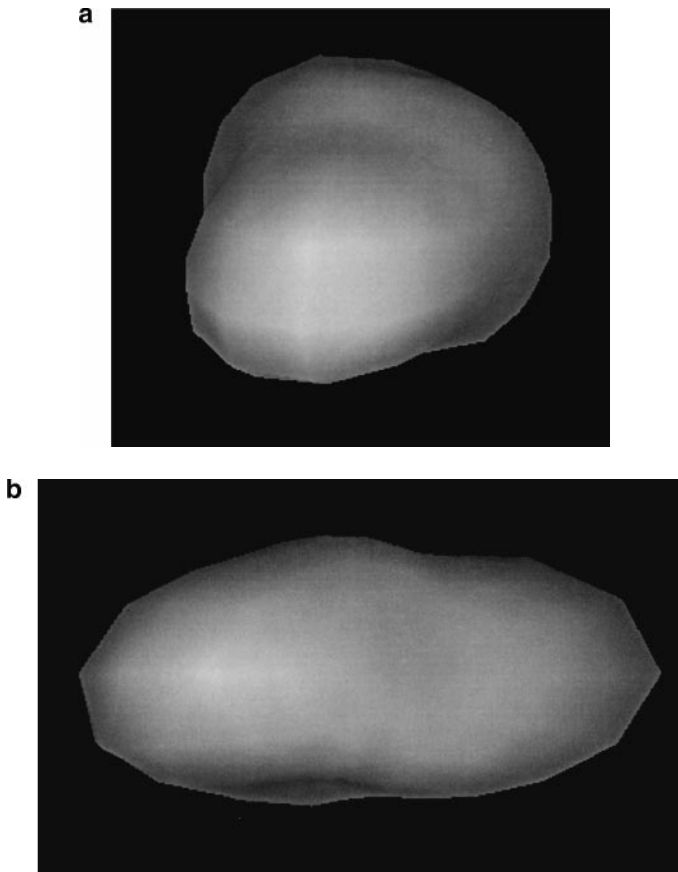


**FIG. 13.** Nonconvex shape model of 243 Ida, seen and illuminated from two directions:  $(\theta, \phi) = (20^\circ, 10^\circ)$  and  $(\theta, \phi) = (0^\circ, 240^\circ)$ .

model and thus describe the probable nonconvex fluctuations of the body. The early truncation point is essential, as discussed in Paper I.

Can nonconvex models be trusted at all then? In principle the reliability conditions are quite obvious: at least as good a  $\chi^2$  as that of the convex model, and the same major surface features from different initial values and regularization strengths. In practice, these conditions typically seem to be fulfilled no better than moderately well. But since we know that asteroids are not convex, a nonconvex model fitting the data as well (and with some persistent features) as a convex one is certainly an interesting possibility—even if the (necessarily artificial) convex model reproduces all the features seen in the lightcurves.

### 5. CONCLUSIONS, FUTURE PLANS, AND EXHORTATION

To sum up, the recipe for asteroid lightcurve inversion is as follows:

1. Determine the sampling interval of the period from the separation between the local  $\chi^2(P)$  minima by using (2) or by plotting  $\chi^2(P)$  using, e.g., an ellipsoidal model (neither the ratios of the axes nor the pole need to be accurate for this purpose).

2. Choose the trial set of the initial values of pole and period from a suitable grid and/or a previous model. Choose the scattering law and its initial parameters. If the initial shape is not a sphere, use a suitable  $\phi_0$  as discussed in conjunction with (1).

3. Use the function series method of Paper I, adding pole, period, and scattering parameters to the Levenberg–Marquardt procedure. Try different convexity (and/or scale factor) regularization weights if necessary. Pick the best solution of the set.

4. Refine the shape result by switching to the separate facet method of Paper I, using the facet values from step 3 as the starting point. If there still are unexplained features in lightcurves, use new initial values especially for pole. Nonconvex inversion can also be tried at step 3.

5. If the best solution contains real nonnegligible residual nonconvexity, separate the shape solution and albedo asymmetry using convexity constraint (and smoothness regularization) as shown in Paper I.

6. Plot the scale factors to determine the solar phase function  $f(\alpha)$ . Plot the reference phase curve  $\mathcal{R}(\alpha)$ .

7. Find the shape from the facet areas by Minkowski minimization (Paper I).

8. Repeat steps 2–7 with different (but nearby) initial values and scattering laws to obtain error estimates and  $\Delta\rho$  of (5).

We stress the fact that this approach is completely self-contained and independent of other methods; however, prior results are very useful as initial guesses. The procedure is quite simple and automatic since it is general rather than based on modifications of some model types.

It is clear that asteroid lightcurves contain a wealth of “robust” information about the object’s overall shape and rotational state. Indeed, Russell’s early paper (1906), often erroneously thought of as somehow proving detailed asteroid lightcurve inversion almost impossible, has today little more than historical interest. Even very complex lightcurves can be modeled easily and consistently using convex inversion. If the data sets covers sufficiently many geometries, the resulting pole, period, and shape solutions are stable regardless of noise or the scattering law(s) used. The potential insufficiency of the data shows during the inversion procedure; even large data sets may not be as informative as smaller but more varied ones. Often the pole and the period can still be expected to be accurate even if no details can be obtained for the shape.

It is rather surprising how minimal the fingerprints of even large concavities are in lightcurves. The weak effect of macroscopic nonconvex features even at large solar phase angles may seem even counterintuitive at first: after all, the shadows are clearly visible in any disk-resolved probe or simulation images. The paradox is solved by two things: the smoothing property of lightcurves (doubled for reference phase curves) and the fact that the inversion results is a photometric rather than geometric convex hull of the body. As our inversion results and simulations

show, the explanatory power of such convex shapes is quite remarkable.

It is also clear that the role of the scattering model is very minor (as long as the model is realistic). Our simulations and real data thus confirm the similar conclusions of Karttunen and Bowell (1989). To put it in a nutshell, pole, period, and the photometric convex hull of the object overwhelmingly dominate lightcurve morphology. Concavities and scattering properties are, in a way, comparable to noise: even though changing them does change the lightcurves somewhat in the direct problem, the solution of the inverse problem does not change much since there are no notably different convex shapes that could model the lightcurves better. The well-posedness and stability of the inversion procedure is thus a result of the convex formulation. The decoupling of the free parameters is remarkably distinct: lightcurves are dictated by rotation and shape, whereas (reference) phase curves are determined by the scattering properties.

We are now in the process of going systematically through the UAPC data base, and it is our purpose to publish a collection of analyses of several asteroids in the near future. It is our intention to build a Web page that would show the results so far, list the asteroids of which observations would be needed the most, and contain a standard report form to be used by observers. We take this opportunity to encourage observers to acquire more lightcurves of good quality: detailed information is vital for proper analysis, whereas poor data are not only worthless but harmful. We would also like to stress that lightcurves with only a few points are usually made in a hurry and under poor conditions and thus belong to the latter category. Near-Earth asteroids are especially rewarding targets: a good coverage of one apparition can produce a detailed model in just a few months.

There are currently no practical scattering laws for the full Stokes vector of light describing both the brightness and the state of polarization. Moreover, polarimetric lightcurve observations, as compared to photometric ones, are still at an early stage of development (see, e.g., Cellino *et al.* (1999)). Solving the inverse problem for the Stokes vector will thus remain an important observational and theoretical challenge. It is quite plausible that, combined with the photometric procedure, polarimetric lightcurve observations can be fully utilized to derive small-scale physical characteristics of asteroid surfaces.

## APPENDIX

### 5.1. Invariant Shapes of Reference Phase Curves

The integrated brightness of a convex body can be written as (see Kaasalainen *et al.* (1992))

$$L(\alpha, \gamma, \theta, \varphi) = \sum_{lm} g_{lm} \sum_{km'} d_{km'}^{(l)}(\gamma) d_{m'm}^{(l)}\left(\theta - \frac{\pi}{2}\right) e^{-im'\pi/2} e^{im\varphi} I_{ik}(\alpha), \quad (6)$$

where the angles  $\alpha$ ,  $\gamma$ ,  $\theta$ , and  $\varphi$  are, respectively, the solar phase, obliquity, aspect, and rotational phase;  $g_{lm}$  are coefficients describing the curvature function of

the body;  $d_{m'm}^{(l)}$  are the rotation matrices of spherical harmonics  $Y_l^m$ ; and

$$I_{ik}(\alpha) = \int_{\alpha}^{\pi} \int_0^{\pi} S'(\vartheta, \psi, \alpha) Y_l^k(\vartheta, \psi) \sin\vartheta \, d\vartheta \, d\psi, \quad (7)$$

where  $S'(\vartheta, \psi, \alpha)$  gives the scattering law  $S(\mu, \mu_0, \alpha)$  in the form in which  $\mu$  and  $\mu_0$  have been replaced by the identities

$$\mu = \sin\vartheta \sin\psi, \quad \mu_0 = \sin\vartheta \sin(\psi - \alpha). \quad (8)$$

In the equatorial reference geometry  $\gamma = 0$  and  $\theta = \pi/2$ , so we have  $d_{km'}^{(l)}(0) \equiv \delta_{km'}$  and  $d_{m'm}^{(l)}(0) \equiv \delta_{m'm}$ . Averaging the brightness over the rotational phase results in yet another Kronecker delta  $\delta_{m_0}$  (i.e., the shape of the body can affect the phase curve only via the latitudinal direction), so the reference phase curve  $\mathcal{R}(\alpha)$  is simply given by

$$\mathcal{R}(\alpha) = \frac{1}{2\pi} \sum_l g_{l0} I_{l0}(\alpha) \quad (9)$$

Further inspection shows that even the remaining influence of  $g_{l0}$  is very restricted.

If the scattering law is suitable,  $I_{l0}(\alpha)$  is separable into single integrals over  $\psi$  and  $\vartheta$ , the index  $l$  (i.e., shape dependence) being associated with  $\vartheta$ , and  $\alpha$ -dependence with  $\psi$ . Thus, for example, geometric scattering (not to be used in any realistic studies) always produces reference phase curves shaped as  $\mathcal{R}(\alpha) = a(1 + \cos\alpha)$ , i.e., in magnitudes  $b - 2.5 \log(1 + \cos\alpha)$ , where  $a$  or  $b$  is a constant depending on the size and shape of the body.

If the scattering law is of the form (3), we obtain

$$\mathcal{R}(\alpha) = f(\alpha)[ck_L f_L(\alpha) + k_{LS} f_{LS}(\alpha)], \quad (10)$$

where  $k_L$  and  $k_{LS}$  are shape-dependent constants (the latter equal to  $a$  of geometric scattering), and  $f_L(\alpha)$  and  $f_{LS}(\alpha)$  are the invariant shapes of the phase curves given by, respectively, Lambert and Lommel–Seeliger scattering. The constant  $k_{LS}$ , for example, is given by

$$k_{LS} = \sum_l h_l g_{l0}, \quad (11)$$

where the coefficients  $h_l$  are nonzero only for even  $l$  and decrease very rapidly: at first by an order of magnitude between  $l$  and  $l + 2$ , and then asymptotically  $l + 5$ -fold. The form (3) resembles the more complicated and inseparable Hapke or Lumme–Bowell models; thus, taking into account the convergence of  $g_{l0}$  and the fact that  $f_L(\alpha)$  and  $f_{LS}(\alpha)$  are not very different when  $\alpha < \pi/2$ , we have an analytical result supporting the numerical conjecture that the shape of a body affects its reference phase curve very little.

## ACKNOWLEDGMENTS

We thank Jukka Piironen for assistance with the UAPC lightcurve data base, and the reviewers, Edward Bowell and Scott Hudson, for valuable comments and questions. Research funded, in part, by the Academy of Finland.

## REFERENCES

- Bowell, E., B. Hapke, D. Domingue, K. Lumme, J. Peltoniemi, and A. W. Harris 1989. Application of photometric models to asteroids. In *Asteroids II* (R. P. Binzel, T. Gehrels, and M. S. Matthews, Eds.), pp. 524–556. Univ. of Arizona Press, Tucson.
- Cellino, A., R. Gil Hutton, E. F. Tedesco, M. Di Martino, and A. Brunini 1999. Polarimetric observations of small asteroids: Preliminary results. *Icarus* **138**, 129–140.
- Hudson, R. S., and S. J. Ostro 1999. Physical model of Asteroid 1620 Geographos from radar and optical data. *Icarus* **140**, 369–378.

- Hudson, R. S., and 26 colleagues 2000. Radar observations and physical model of Asteroid 6489 Golevka. *Icarus* **148**, 37–51.
- Kaasalainen, M. Interpretation of lightcurves of precessing asteroids. *Astron. Astrophys.*, in press.
- Kaasalainen, M., and J. Torppa 2001. Optimization methods for asteroid lightcurve inversion. I. Shape determination. *Icarus* **153**, 000–000.
- Kaasalainen, M., L. Lamberg, K. Lumme, and E. Bowell 1992. Interpretation of lightcurves of atmosphereless bodies. I. General theory and new inversions schemes. *Astron. Astrophys.* **259**, 318–332.
- Kaasalainen, M., K. Muinonen, and T. Laakso 2001. Shapes and scattering properties of large irregular bodies from photometric data. *Optics Express* **8**, 296–301. [Available at <http://epubs.osa.org/opticsexpress/>.]
- Kaasalainen, S., K. Muinonen, and J. Piironen 2001. A comparative study of the opposition effect of icy solar system objects. *J. Quant. Spect. Rad. Transf.*, in press.
- Karttunen, H., and E. Bowell 1989. Modelling asteroid brightness variations. II. The uninterpretability of light curves and phase curves. *Astron. Astrophys.* **208**, 320–326.
- Lagerkvist, C.-I., P. Magnusson, I. Befskeya, J. Piironen, J. Warell, and M. Dahlgren 1996. *Asteroid Photometric Catalogue*, fourth update. Uppsala Univ. Press, Uppsala.
- Lagerkvist, C.-I., and J. Piironen 2001. *Asteroid Photometric Catalogue*, fifth update. Uppsala Univ. Press, Uppsala.
- Mottola, S. A., and 27 colleagues 1997. Physical model of near-Earth asteroid 6489 Golevka (1991 JX) from optical and infrared observations. *Astron. J.* **114**, 1234–1245.
- Muinonen, K. 1994. Coherent backscattering by solar system dust particles. In *IAU Symposium No. 160, Asteroids, Comets, Meteors 1993* (A. Milani, M. Di Martino, A. Cellino, Eds.), pp. 271–296. Kluwer Academic, Dordrecht.
- Russell, H. N. 1906. On the light-variations of asteroids and satellites. *Astrophys. J.* **24**, 1–18.
- Simonelli, D. P., J. Veverka, P. C. Thomas, and P. Helfenstein 1995. Analysis of Gaspra lightcurves using Galileo shape and photometric models. *Icarus* **114**, 387–402.
- Simonelli, D. P., J. Veverka, P. C. Thomas, P. Helfenstein, and B. T. Carcich 1996. Ida lightcurves: Consistency with Galileo shape and photometric models. *Icarus* **120**, 38–47.
- Veverka, J., and 32 colleagues 2000. NEAR at Eros: Imaging and spectral results. *Science* **289**, 2088–2097.